Widespread flooding dynamics changing under climate change: characterising floods using UKCP18

Adam Griffin[1], Alison Kay[1], Paul Sayers[2], Victoria Bell[1], Elizabeth Stewart[1], Sam Carr[2]
[1]UK Centre for Ecology & Hydrology, Wallingford, Oxfordshire, OX10 8BB, UK.
[2]Sayers and Partners, Watlington, Oxfordshire, OX49 5PY, UK.

Correspondence to: Adam Griffin (adagri@ceh.ac.uk)

Abstract. An event-based approach has been used to explore the potential effects of climate change on the spatial and temporal coherence of widespread flood events in Great Britain. Time series of daily mean river flow were generated using a gridded national-scale hydrological model (Grid-to-Grid) driven by the 12-member ensemble of regional climate projections from UK Climate Projections 2018 (UKCP18). Gridded flow series were generated nationally for 30-year baseline (1980-2010) and future (2051-2080) time-slices from which sets of widespread extreme events were extracted. These events were defined as exceeding an at-site 99.5th percentile (equivalent to two days per year) simultaneously over an area of at least 20 km^2, with a maximum duration of 14 days. This resulted in a set of 14,400 widespread events: approximately 20 events per year, per ensemble member, per time-slice. Overall, results have shown that events are more temporally concentrated in winter in the future time-slice compared to the baseline. Distributions of event area were similar in both time-slices, but the distribution of at-site return periods showed some heavier tails in the future time-slice. Results were consistent across ensemble members, with none showing significant difference in distribution.

1 Introduction

According to the 2020 UK National Risk Register (HM Government, 2020), river flooding is one of the highest impact hazards affecting the UK. Flood prediction, and more generally flood frequency estimation, is crucial to mitigating these hazards to reduce impact. Flood frequency estimation is often carried out on a single-site basis, computing the frequency of floods at specific locations in isolation. However, the management of flood risk on a regional or national basis requires an understanding of how likely it is that multiple locations will experience floods at the same time. Widespread flooding presents a huge challenge for local communities and emergency response services and has long-lasting impacts, as demonstrated by the extensive flooding experienced in North-West England as a consequence of Storm Desmond and Storm Frank in winter 2015/2016 (Barker et al., 2016).

One approach to risk quantification is catastrophe modelling (CAT modelling), which is used in the insurance industry to assess annual average losses. CAT modelling typically makes use of three components: property data, stochastic hazard event sets and a relationship between magnitude of hazard and the expected loss for each property (Grossi and Kunreuther, 2005). The present work focuses on the second component: developing a set of widespread flood events, here characterised by river flow and the probability of exceeding that flow. Simply making use of observed widespread events typically does not provide

enough data to reliably determine hazard probability. Therefore, developing a larger set of events for analysis is desirable to improve the uncertainty of risk estimates, particularly for events which have a return period (or average recurrence interval) greater than the length of observed records. For example, return periods as long as 1 in 200 years are often used as the design standard for large-scale engineering projects. This can involve making use of hydrological models driven by large ensembles of data from climate models (ensembles of model runs using perturbed parameter sets) over a shorter time period (Kelder et al., 2020), or through predominantly stochastic event-based models (Filipova et al., 2019).

Climate change affects flow regimes globally (Jiménez Cisneros, 2015), and studies suggest that flooding in the UK is likely to become (or has already become) more frequent and severe (Collet et al., 2018). Spatial coherence of flooding events – whether flood timings at different locations have become more correlated – is of key interest to national-scale actions to mitigate the associated loss. The dependence structure of river flow has been analysed on a Europe-wide scape (Berghuijs et al., 2019) and for the United States (Brunner et al., 2020), focusing on synchrony of events within a given range. The UK's Third Climate Change Risk Assessment (CCRA3) included work which analysed the changes in risk caused by possible changes in flood dynamics (Sayers et al., 2020). CCRA3 adds to the breadth of guidance that has been developed for policymakers and water managers to try and account for such changes (Reynard et al., 2017).

This paper makes use of the Grid-to-Grid hydrological model (Bell et al., 2009) and the UK Climate Projections 2018 (UKCP18) Regional Projections (Met Office Hadley Centre, 2018b) to generate two sets of over 7000 hazard events for the recent past (1980-2010) and the future (2050-2080). The question of what defines a "widespread flood event" is discussed, and differences between events in terms of extent, likelihood and duration are analysed in the context of possible changes in the spatio-temporal structure of widespread events in the future. Often flooding is considered on a site-by-site or regionally summarised fashion, particularly when looking into projections of the future. This paper hopes to show the benefits of considering widespread flooding events over a large area using gridded, rather than catchment-based hydrological modelling to expand our knowledge of the extent of possible flooding events in the UK. Comparing UKCP18-driven model runs to those driven by observed rainfall and temperature will give confidence to the use of these event sets in future analysis. Note that, within the context of flood frequency, this paper refers to floods or flooding events, although in reality many of these will be merely high flows that do not exceed bankfull.

2 Data

2.1 Climate projections

UK Climate Projections 2018 (UKCP18) provides information on potential changes in a range of climate variables over the 21st century, via a number of different products (Murphy et al., 2018). This dataset has previously been used to analyse river flows in the UK and how they may differ in the future due to climate change (Kay 2021; Kay *et al.*, 2021).

The UKCP18 Regional Projections (Met Office Hadley Centre, 2018b) comprise a 12-member perturbed parameter ensemble (PPE) of the Hadley Centre Regional Climate Model (RCM), nested in an equivalent PPE of their Global Climate Model

(GCM). The ensemble covers the period December 1980 to November 2080 under an RCP8.5 emissions scenario (Representative Concentration Pathway) (Riahi et al., 2011). The 12 ensemble members are numbered from 01 to 15, where 01 uses the "standard" parameterization of the Hadley Centre RCM, and ensemble members 02, 03 and 14 are not available. The rainfall and temperature used in the present work is on a 12 km spatial resolution and a daily timestep covering England, Scotland and Wales for a synthetic 360-day year (30 days per month). The data are available re-projected from the native climate model grid to a 12 km grid aligned with the Great Britain (GB)national grid. The re-projected daily precipitation and daily minimum and maximum temperatures are used in the present work.

3 Methods

3.1 Hydrological model

The Grid-to-Grid (G2G) hydrological model employs digital datasets to simulate the natural flow response to rainfall across the model domain. In this study, G2G was implemented as an area-wide runoff-production and flow routing model, producing outputs on a 1km grid aligned with the GB national grid (Bell et al., 2009). G2G makes use of the UK 50m Integrated Hydrological Digital Terrain Model (IHDTM; Morris and Flavin, 1990) to derive high resolution river networks and terrain information. The network-derivation scheme of Paz et al. (2006) was used to identify 1km-resolution flow directions from hydrologically-corrected 50m river networks, following Davies and Bell (2008). The routing component of G2G applies schemes that invoke the kinematic wave approximation as their basis (Bell et al., 2007a, b). In urban and suburban areas, identified through the LCM2000 spatial dataset of land-cover (Fuller et al., 2002), responsiveness is increased through the use of an enhanced routing speed and reduced soil storage, leading to a faster response to rainfall. Grid-to-Grid has been widely tested and applied to explore climate change impacts on river flows across GB, for both floods (Bell et al., 2009, 2012; Kay et al., 2018) and droughts (Rudd et al., 2019; Kay, 2021; Lane and Kay, 2021). It has also been used by the English Environment Agency for flood forecasting (Price et al., 2012).

This application of G2G used gridded precipitation, temperature and potential evaporation provided either by observations, or from the UKCP18 Regional Projections outlined above as inputs.

An investigation was undertaken to identify whether bias correction should be used in this paper. G2G outputs based on the UKCP18 RCM ensemble members was compared to daily mean flow (data available from the NRFA). The 50-year event (annual exceedance probability of 2%) was calculated for the station and the relevant gridsquare it lies in. Figure 1 shows that across most of Great Britain where the mode was run, bias correction led to a fairly constant underestimation of the 50-year event compared to those from observations. Although the results without bias correction are more variable with some stations showing a large overestimate, they have a better mean bias when calculated nationally, which was felt to be important when looking on a national scale. This was also computed for the 2-year flood with very similar results. Due to this, it was decided that bias correction would not be applied in this paper.

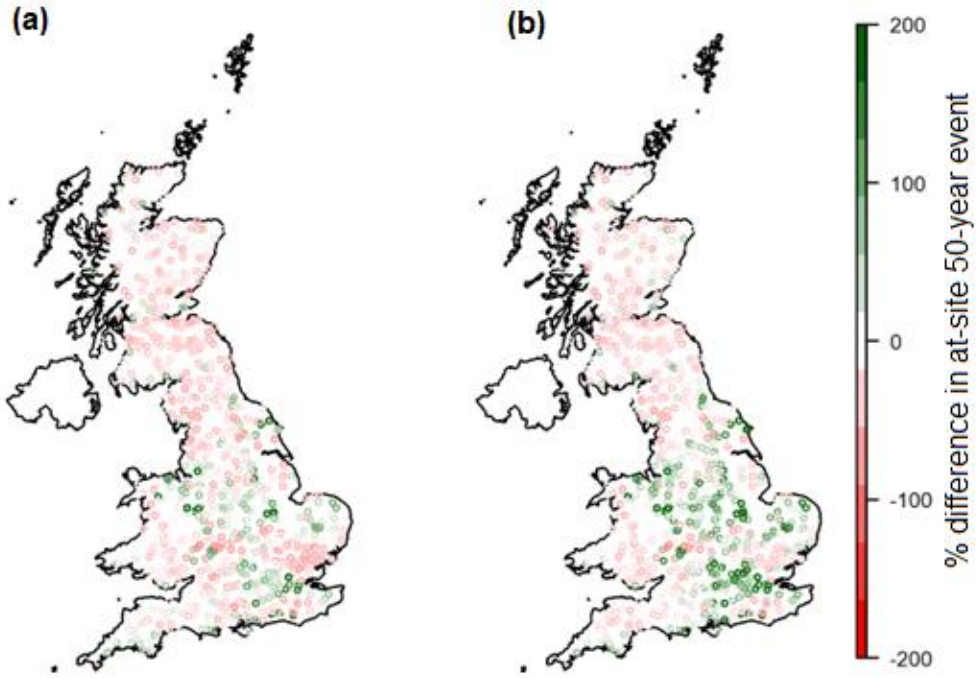

Figure 1 Comparison of difference between (a) with and (b) without bias correction averaged over all 12 ensemble members. Colour indicated the change between the estimate for the 50-year return period peak flow (based on gauged daily flow). Positive values indicate that modelled data has a larger value of Q50.

In isolation it is difficult to say whether these results are realistic compared to observations. However, gridded river flow observations are not available for Great Britain nationally. Therefore, in addition to the UKCP18-driven G2G output, this paper also presents data from a set of "observation-based simulations" as used in Kay (2022; Fig 1) as a step towards comparing modelled and observed extreme flow. This run still uses Grid-to-Grid but is driven using observed inputs: CEH-GEAR daily gridded precipitation (Tanguy et al., 2016), monthly short grass potential evapotranspiration (40km resolution) from MORECS (Hough and Jones, 1997), and daily 1km minimum and maximum daily temperatures (Met Office et al., 2019). Precipitation was subdivided uniformly through the day, and temperature varied sinusoidally between the extremes. In this paper, this will be referred to as the SIMOBS run.

3.2 Event extraction

For each RCM ensemble member, two time-slices were considered: 1980-2010 and 2050-2080, to serve as baseline and future viewpoints. Event time series were extracted using a peak-over-threshold (POT) approach as used by the NRFA (UK National River Flow Archive; Robson and Reed, 1999). In this approach, peaks are identified as exceedances above some predetermined threshold. To improve the independence of events, they must be sufficiently far apart (based on the average time-to-peak of storm hydrographs). Additionally, consecutive events are checked to see if the minimum flow between the two peaks is less than two-thirds of both peaks, otherwise the lower peak is discarded (this process is iterated until no more events are removed).

To determine the most appropriate exceedance threshold to use at each 1km grid-square, five different percentiles of flow were investigated, ranging from five events per year to one event every 10 years on average. As a result, for each grid-square the following numbers of days were selected for each time-slice:

- 5 events per year (POT5) – 148 days per grid-square
- 2 events per year (POT2) – 60 days per grid-square
- 1 event per year (POT1) – 30 days per grid-square
- 1 event in 5 years (POT0.2) – 5 days per grid-square
- 1 event per decade (POT0.1) – 3 days per grid-square

Note this is independent of the distribution of the data due to the use of empirical percentiles rather than fixed, absolute values of flow.

We define widespread events as timepoints for which a large number of locations experience very high flow (i.e. above the POT threshold) simultaneously. To determine when widespread events occurred, different levels of extent above threshold were investigated to ensure that a good range of widespread events were captured, whilst ensuring that only events that could be described as "extreme" in some way were retained. To this end, the extent of an event was measured by the percentage of grid-squares on the river network which were simultaneously above their respective threshold values (denoted "inundated").. Five minimum extents were investigated: 5%, 2%, 1%, 0.5%, and 0.1%. Note that for the GB river network, 19,914 grid-squares were considered as being in the network, so an extent of 1% corresponds to ~200 km^2 of inundated grid-squares.

To select the at-site threshold and minimum extent, all the combinations above were trialled on a single ensemble member (01) for the 1980-2010 time-slice, and the number of days fulfilling both inundation criteria (at-site threshold and minimum extent) over the 30-year time-slice are shown in Table 1. Very similar patterns of events extracted (not different at a statistically significant level) were observed for all of the ensemble members.

Table 1 Number of days where national inundation according to a given threshold (rows) exceeds a certain percentage (columns). PoE = Daily Probability of exceedance

		Extent lower threshold				
# exceedences	**Daily PoE**	**5%**	**2%**	**1%**	**0.5%**	**0.1%**
POT5	5/360	839	1510	1981	2418	3427
POT2	2/360	353	727	1027	1340	2031
POT1	1/360	160	401	589	826	1345
POT0.2	1/720	25	77	144	239	444
POT0.1	1/3600	14	35	74	117	262

The POT2 threshold and the 0.1% minimum extent were selected for the following reasons. POT2 provided a good balance between having enough exceedances to derive widespread events and keeping the threshold high enough to reasonably model

the peaks-over-threshold using an extreme-value distribution. The 0.1% inundation coverage was selected to ensure that small, very extreme events were not excluded.. For applications in risk estimation, these events of smaller extent may occur in areas with high potential economic losses, and so are important for accurately estimating national annual damages.

With this set of parameters for inundation, the specific at-site thresholds were calculated for each grid-square under each RCM ensemble member, using the thresholds from the 1980-2010 time-slice for both baseline and future events. This was to allow the future events to be described in terms of baseline return periods.

At this point, the event set consisted only of single-day events, which may not truly represent widespread events in the temporal sense, owing to the way in which storms move across a region over time and the typical time taken for water to travel downstream. To correct this, multi-day events were also defined. For the selected inundation threshold (POT2), event lengths were defined as the number of consecutive days for which the extent exceeded the selected spatial limit (0.1%). For the RCM 01 ensemble member in the 1980-2010 time-slice, the distribution of event lengths is shown in Fig 2.

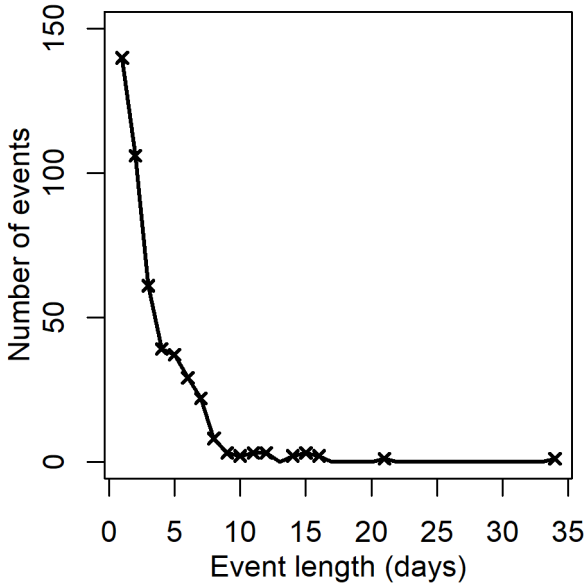

Figure 2 Number of events with different durations, based on 0.5% coverage and at-site exceedance of two days per year.

Here it can be seen that beyond seven days, there are very few events which fall under the definition above. There are some arguments that one should consider events up to 21 days (De Luca, 2017) but this may lead to a greater likelihood of two independent events of small geographical spread being recorded as a single, larger event. Such pairs (or larger groupings) of events may arise from different weather systems in, for example, the North-West and South-East of England. As a compromise therefore, events were limited to 14 days. If an event exceeded this time limit, the 14 days surrounding the day at which spatial spread was highest were retained as “the event” (six before, seven after).

To keep the events simple to interpret, multi-day events were summarised. For each grid-square, each event was summarised by the highest single-day value at that grid-square during that event. Taken nationally, this retains the maximum flow at each

point over the whole region, which should capture the most extreme flows within an event, and will also be helpful for estimating upper bounds of risk associated with such events. A more in-depth investigation into multi-day events could be the focus of future work.

To assess the change in spatial extremal datasets, one can investigate whether the spatial dependence changes between time-slices; χ and $\bar{\chi}$, two measure of extremal dependance (Coles, 2001), are calculated between pairs of points. $\bar{\chi}$ describes the level of asymptotic independance between two random variables if both are above given thresholds. χ complements this: if two random variables are asymptotically dependent, this describes the strength of that asymptotic dependence. For two points i and j,

$$\chi_{i,j} = \lim_{x \to \infty} P[Q_i > x | Q_j > x]$$

If $C^*(u,v) = 1 - u - v + C(u,v)$, for a copula C, then

$$\bar{\chi} = \lim_{u \to 1} \frac{2 \log (1-u)}{\log C^*(u,u)}$$

χ describes the level of asymptotic dependence; if $\chi > 0$ then the variables are asymptotically dependent, and $\bar{\chi} = 1$ automatically. But if $\chi = 0$, they are asymptotically independent. In this case, $\bar{\chi}$ describes the dependence for large but not asymptotic values of flow. $\bar{\chi}$ close to 1 indicates the variables are highly dependent except at the asymptotic limit.

3.3 Return Periods

To ensure a good fit of return periods for the most extreme events, the top 60 independent peaks in each ensemble member and timeslice were found using the peak-extraction algorithm as described in Section 3.2. For values over the threshold, a Generalised Pareto distribution (GPa) was used with distribution function

$$F_{GPA}(x) = 1 - \left(1 + \frac{\kappa(x-u)}{\alpha}\right)^{\frac{1}{\kappa}} = P[Flow > x | Flow > u]$$

with threshold u, scale parameter $\alpha > 0$ and shape parameter $-1 \leq \kappa \leq 1$. This was fitted to the series of independent peaks over the threshold to give a modelled daily probability of exceedance. u is the flow threshold at a specific location, and $P[x > u] = 2/360$, since this investigation uses the POT2 threshold defined in Section 3.2.

To convert from a per-exceedance PoE to a more widely-used annual PoE, a simple scaling factor was applied based on there being 60 events per location over 30 years:

$$p_{ANNUAL} = p_{EVENT} \times \left(\frac{60}{30}\right)$$

In the rest of this work, plots are presented using annual probabilities of exceedance. Due to the limits of using 30-year time-slices of data, return periods are capped at 1000 years since the uncertainty on exceedance probabilities is very high for the most infrequent events.

4 Results

Fig 3 shows four example events extracted from the 1980-2010 time-slice from RCM ensemble member 01, with return periods described in years. The coloured extent of an event was restricted to those points with a daily probability of exceedance of less than 2/360. The percentages shown refer to the percentage of the number of river grid cells, not a fraction of UK land area.

On the whole, the events are spatially contiguous, and the example events suggest that return period is highly peaked around one location and quickly tapers off away from the "epicentre". These are four of the largest events in the 1980-2010 time-slice and show a broad range of different events covering Scotland, southern England and central England, with key patches of very extreme flow in Fig 3b, Fig 3c and Fig 3d, whereas Fig 3a shows a widespread but less severe event (in terms of return period of flow). In the rest of this section, return periods reported in the text and figures are the maximum return period observed (across space and time) within a single event.In this paper, analysis focuses on the differences between past and future and across space, though differences between the RCM ensemble members should be mentioned. Fig 4 shows that the event areas are fairly consistent between the RCM-driven runs and the SIMOBS run, with a slight bias in the RCM-driven runs to larger events with lower return periods All the RCM-driven runs show a slightly flatter distribution of return periods in the 2050-2080 time-slice. Supplementary Material Fig 1 shows how the results vary between ensemble members. Ensemble members 07 and 08 shows a slightly more uniform distribution of events across log(Area), and ensemble member 11 shows a slightly higher number of small events, around 200 events with a footprint of less than 100km^2. Ensemble member 01 shows the greatest difference between the 1980-2010 and 2050-2080 time-slices (more than 50 fewer events with return period less than 8 years)In the rest of this section, the event sets from all ensemble members are combined and given equal weighting. In the supplementary material, ensemble members are treated as separate sources of equal weighting. Ensemble members are shown in different colours and have the convex hull of the points from each ensemble member highlighted to show in particular variation in the extremes.

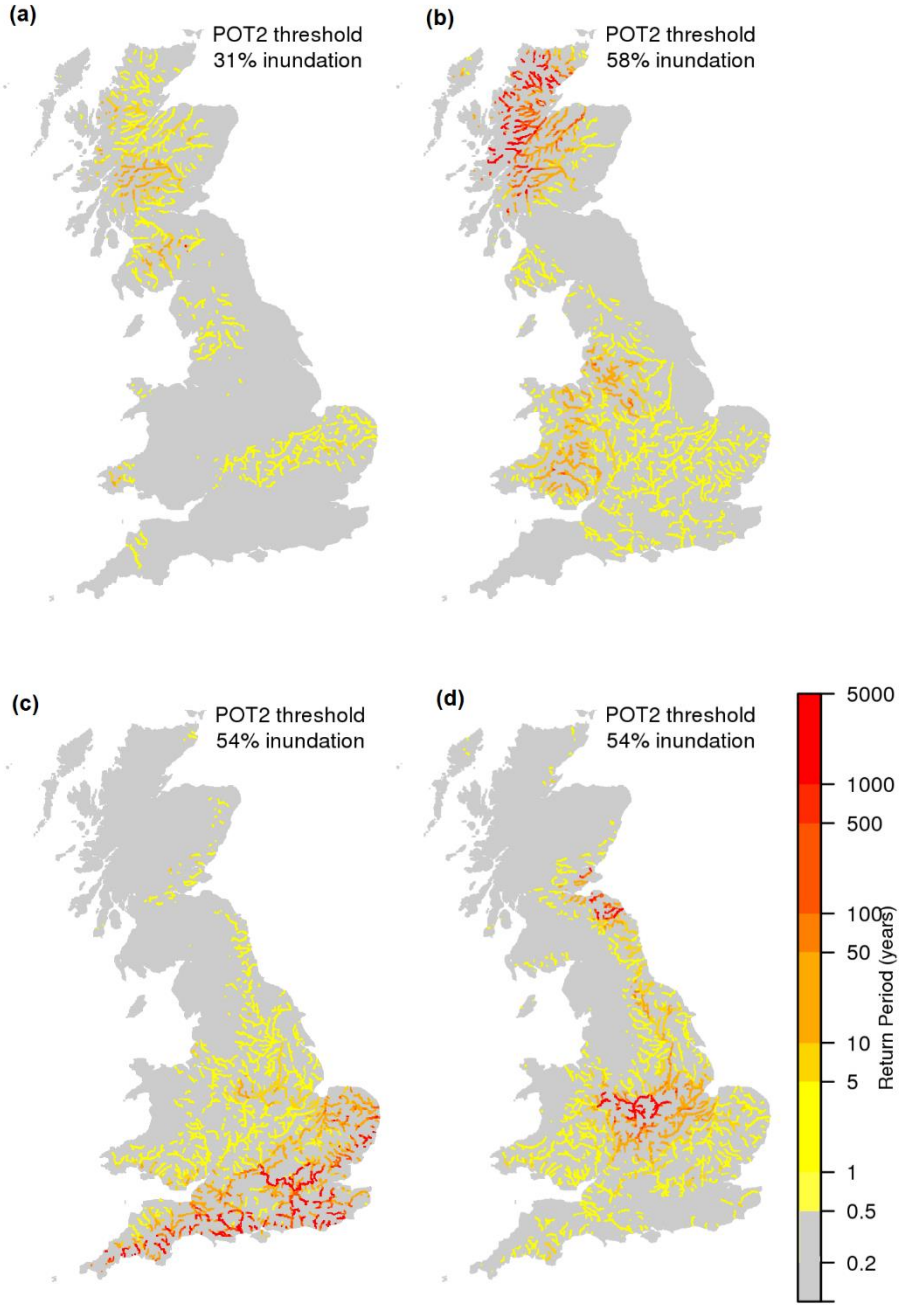

Figure 3 Example events from 1981-2010 time-slice from a single RCM ensemble member, showing return period in years.

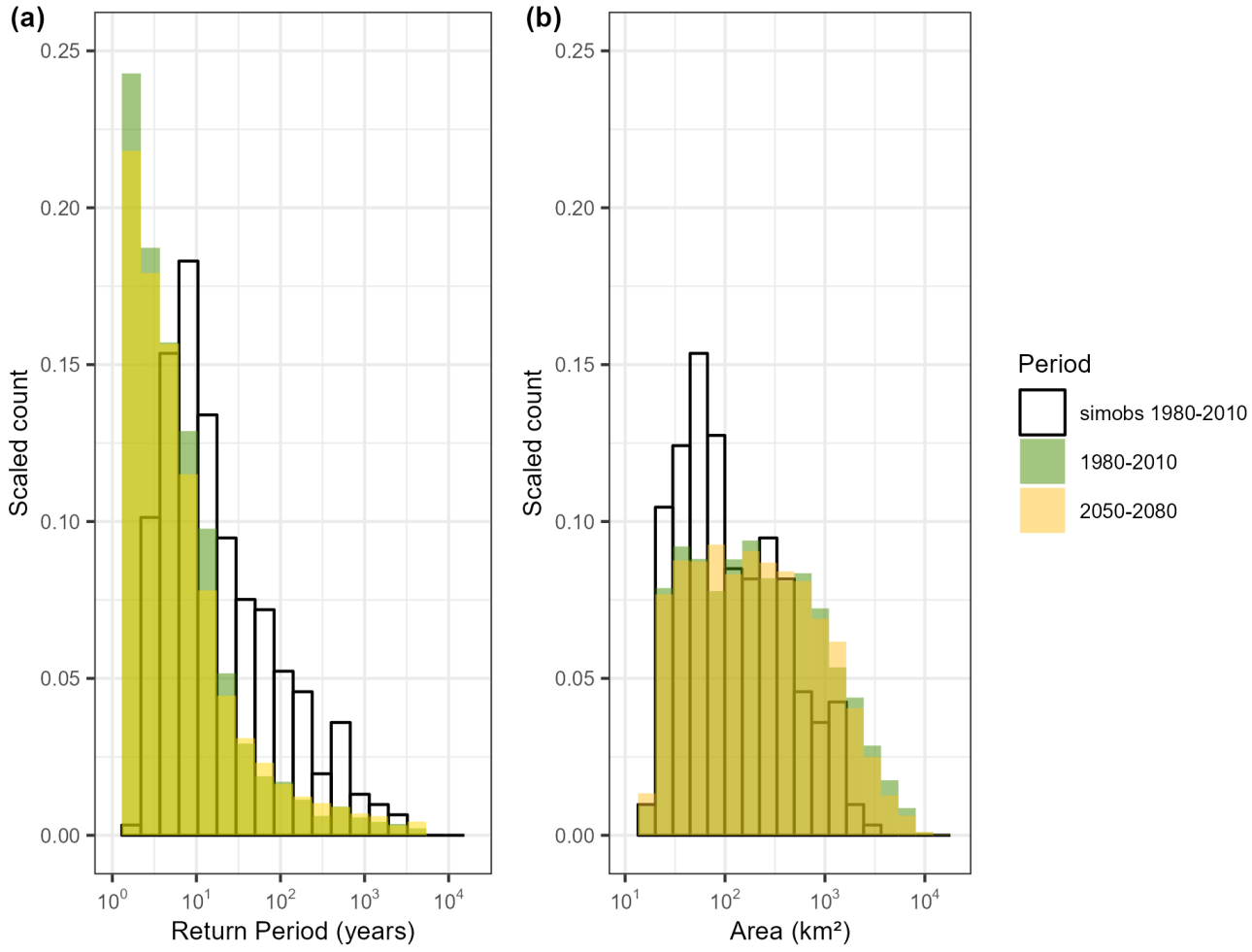

Figure 4 Histograms showing distribution of event area and return period, split across time-slices.

Taking the union of events extracted from all the ensemble members, changes in extent and duration can be examined. Figure 5 highlights the changes in the number of widespread events between the two time-slices, subdivided by boreal season. The figure shows overall more widespread events in the future (7553) than in the 1980-2010 time-slice (7225 events). However, in the months of March to August, and particularly in June to August (boreal summer), one sees fewer widespread events in the future time-slice.

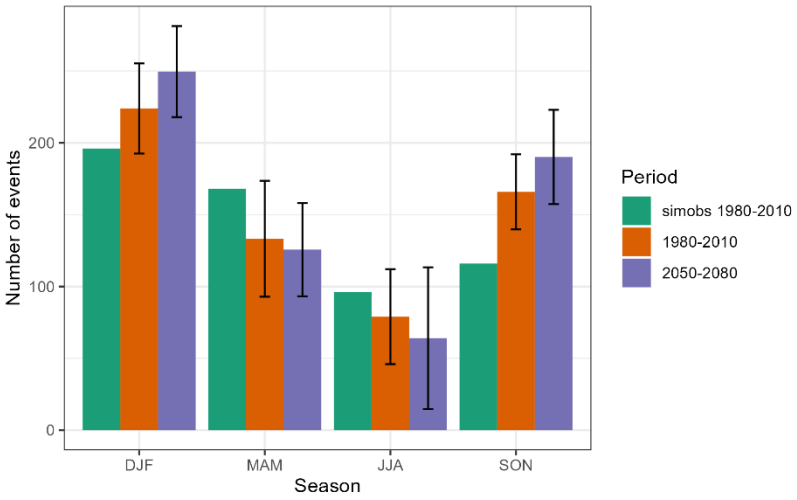

Figure 5 Number of widespread events, summed across ensemble members, split by season and time-slice. Left: total events, Right: mean number of events per ensemble member with error bars showing minimum and maximum across ensemble members.

In terms of event duration, Fig 6 shows how this varies by season and time-slice, and how that is linked to return period. The SIMOBS run appears to generate shorter events on average compared to the RCM-driven runs, suggesting a slightly stronger temporal autocorrelation in the effects of the use of UKCP18 input data. The return periods (as seen in Figure 3) are broadly similar in distribution. The figure suggests that duration and return period are somewhat correlated, in that the longest duration events are very unlikely to have a low return period (i.e. to occur frequently). However, there are a number of events which are of short duration but high return period. As one might expect, events are shorter in boreal summer (JJA), with very few summer events extending longer than 5 days. In the future time-slice, event duration seems to be slightly shorter on average, and this is more pronounced in spring (MAM) and summer (JJA) , reducing from 3.54 to 2.99 days in spring, 2.20 to 2.04 in summer. The events with the highest return periods are in boreal autumn (SON) and winter (DJF), in both time-slices, though the distribution of return periods in the future has heavier tails (note the return period axis is on a logarithmic scale). Supplementary material figure 1 shows that there is some variability between ensemble members, particularly in the extremes, but the overall pattern is preserved throughout, as expected from Figure 4.

Figure 6 shows how area and peak return period vary by season in the two time-slices, and in comparison to the SIMOBS run. As one might expect, there is a correlation between area and peak pointwise return period across both RCM-driven time-slices. The changes between the two time-slices are subtle, but there is an overall trend towards an increase in the range of peak return period: the 95th percentile of return periods increases in all seasons, from an increase of 10 years in spring to 205 in summer, with the 5th percentile being ~1.2 in all seasons and timeslices. The extent of widespread events appears to stay consistent between the 1980-2010 and 2050-2080 time-slices, with a possible slight reduction in extent of the largest events in the future summer. We see that in all seasons are a small number of events with return periods exceeding 1000 years, particularly in winter and autumn. Supplementary material figure 3 shows that this pattern is matched between ensemble members, but there is some variability in the relative patterns of duration and rarity in the extremes.The SIMOBS run shows a broadly similar

distribution to the baseline (1980-2010) timeslice, although the variability and reduced smoothness appears to be increased, due to the much smaller number of events from that single run (~500 compared to ~7000 from all 12 RCM ensemble members).

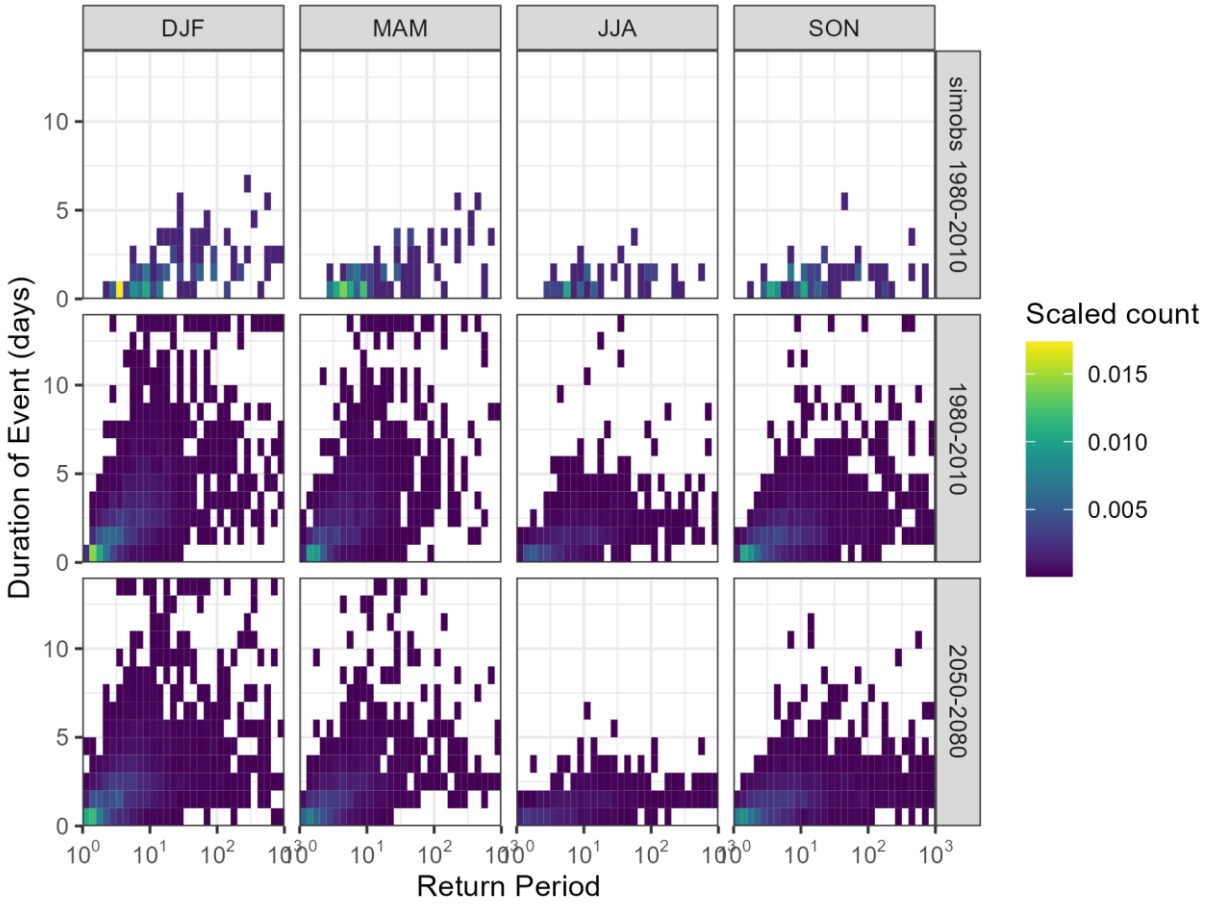

Figure 6 Heatmaps showing joint distribution of return period and event duration, summed across ensemble members, split by season and time-slice. Count is scaled so that the total of events in each timeslice adds up to 1.

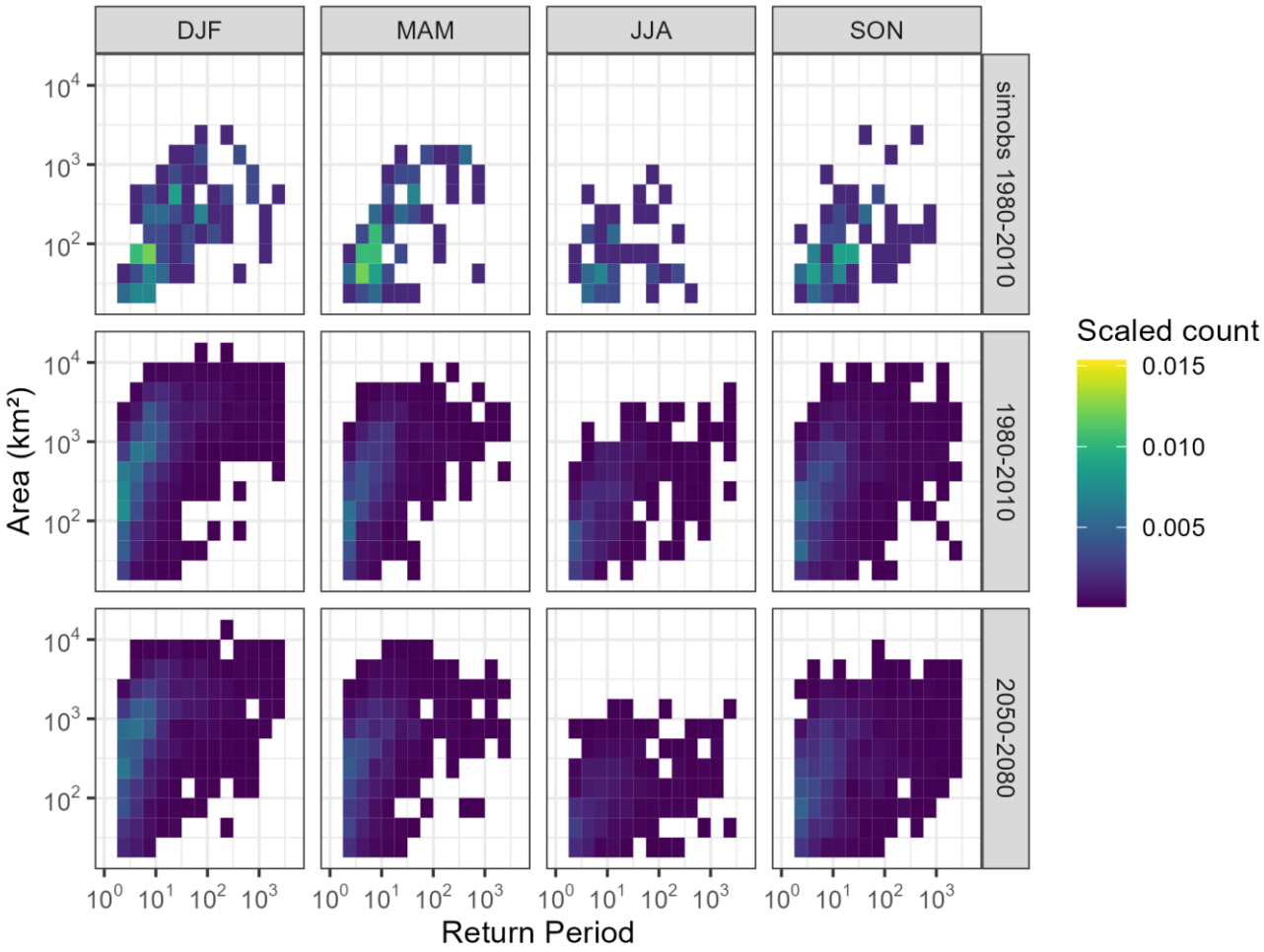

Figure 7 Heatmaps showing distribution of events with different areas and return periods, split by time-slice and season, summed across all ensemble members. Count is scaled so that the total of events in each timeslice adds up to 1.

Figure 8 shows how dependence varies between pairs of points across the river network. Here asymptotic dependence appears to have a limit at most location pairs of around 120km (χ is only shown for pairs of locations for which the upper bound of a bootstrapped uncertainty bound of $\bar{\chi}$ exceeds 0.99). The figure suggests that asymptotic dependence decreases as distance increases. In the asymptotically independent case (Figure 8), we see a similar pattern in dependence for large values of flow, with high dependence at short distances, even if they are independent in the limit.. There seems to be little change in dependence between the two time-slices, although the asymptotic dependence appears to extend slightly further in the baseline time-slice (a maximum distance for which $\bar{\chi} = 0$ of 300km in the baseline versus 260km in the future). If the events are subdivided by season, subtle differences can be observed (Fig 9). Overall, spring and summer shows less asymptotic dependence (lower values of χ and $\bar{\chi}$) than autumn and winter. In spring and summer (Mar-Aug), mean χ is 0.641 and mean $\bar{\chi}$ is 0.222, compared to mean χ is 0.673 and mean $\bar{\chi}$ is 0.363 for autumn and winter (Sep-Feb). Also, the 50% contour for $\bar{\chi}$ is

longer in spring (MAM) (max distance of 495km in baseline, 545km in future) than boreal summer (JJA) (max distance of 431km in baseline, 462km in future) in both time-slices, suggesting that the variance in $\bar{\chi}$ exhibits seasonal variation. Between baseline and future, as for Fig 7, the differences are marginal, but both χ and $\bar{\chi}$ show smaller 50% contours in autumn compared to the other seasons, suggesting reducing variation in asymptotic dependence in this season. For other percentile contours, patterns are very similar and follow the shapes of Fig 8. This is also mirrored in Supplementary material figure 4, which shows this split by ensemble member, where spatial variation in coherence is strongly preserved between ensemble members.

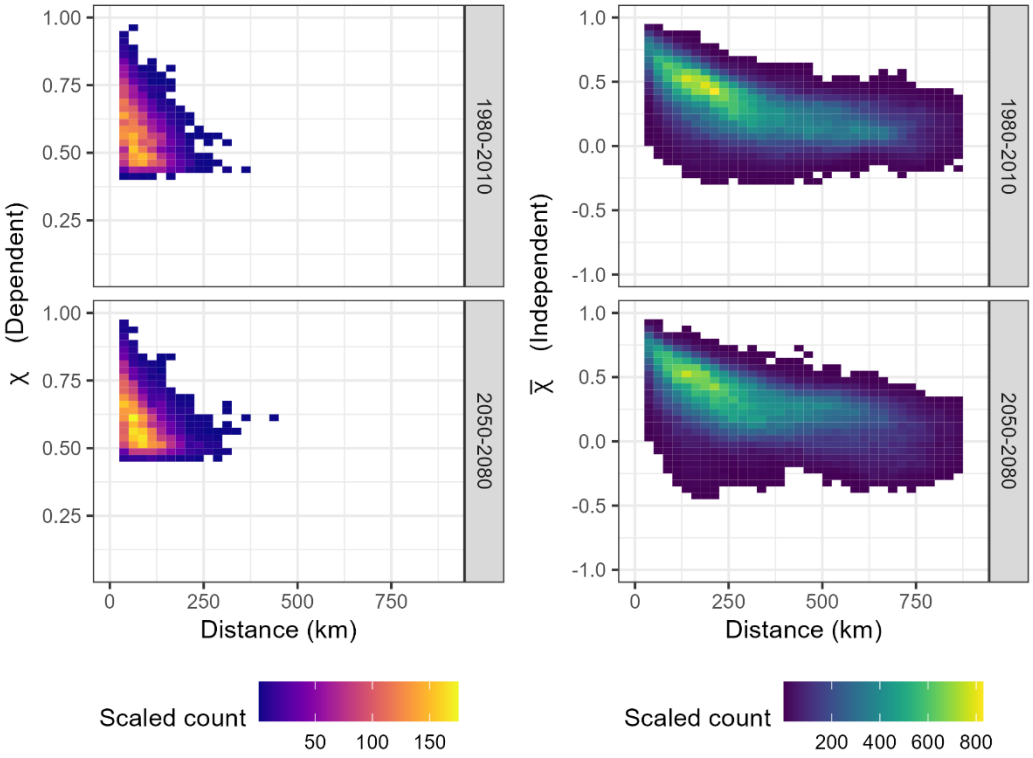

Figure 8 Heatmaps showing asymptotic dependence for 100 000 random pairs of points on the river network. χ is only shown for pairs of locations which are asymptotically dependent based on $\bar{\chi} > 0.99$.

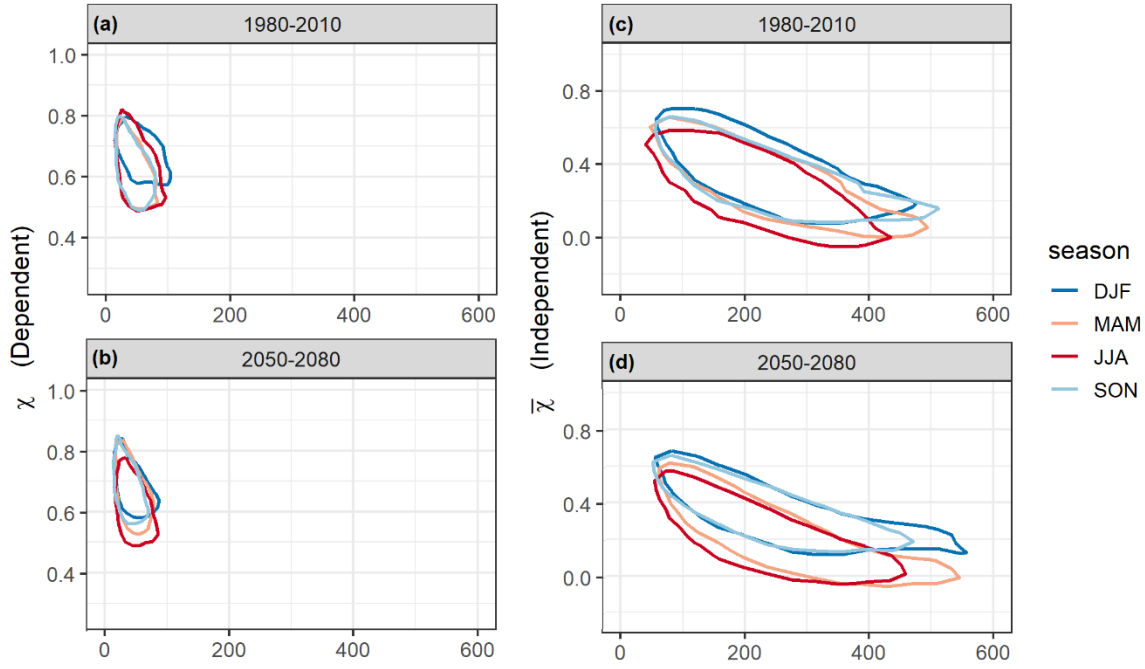

Figure 9 Contour showing asymptotic dependence for 100 000 random pairs of points on the river network. Contours show smallest area that contains 50% of point-pairs, split by season and time-slice. χ and $\overline{\chi}$ as in Figure 7

5 Discussion

The event extraction method did not explicitly require events to be spatially contiguous, but this does generally appear to be the case in the largest events. The event in Fig 3a does suggest that some number of potentially simultaneous but independent events are captured; this may be due to two separate events happening on consecutive days due to the method of event length determination. This suggests that a more sophisticated form of event delineation could improve the process.

A non-trivial number of very extreme events were observed in the RCM-driven runs. Although extreme, Tawn et al. (2018) point out that, within the observed annual maxima series, the chance of a 100-year return period event occuring somewhere within a set of 916 gauging stations in England and Wales is approximately 78%, and so over a gridded dataset of more points, and with more events, the observation of these extremely rare events is statistically plausible. Also, due to the probability distributions used, a small change in event peak flow magnitude in the upper tail of the distribution can lead to a large change in return period (when the shape parameter κ is positive, which is the case for most of the UK (Griffin et al., 2019)).

The number of widespread events (based on a POT2 threshold derived from 1980-2010 data) was found to increase in total in the future time-slice (Fig 5) but was slightly lower in the future for spring and summer (March-August) events. This matches with some work done by Lavers and Villarini (2013) which shows the possible increase in atmospheric rivers, especially in Western Europe, which drive extreme precipitation events. The typical spatial extent of events was found to be fairly consistent between time-slices, but summer (June-August) events appeared smaller in the future across all return periods. Event duration

decreased on average in all seasons between the two time-slices. This pattern was the same across all RCM ensemble members. Kay et al (2022) show that projections of soil moisture changes point towards wetter winters and drier summers. In conjunction with Blöschl et al (2017) suggesting that UK floods are closely linked to soil moisture timing, this gives confidence in the results in the present work. This may suggest a shift to more widespread flooding in boreal winter (DJF), and drier summers (JJA) overall, which lines up with the literature (Murphy et al., 2019). Alternatively, this may instead be linked to a change in the size of flooding events in the future in summer events which, in the UK, are typically linked to short-duration, intense summer storms. Between ensemble members (Supplementary Material Figure 1), variability is higher in boreal summer (JJA), even more so in the future time-slice, and one member actually saw an increase in summer (JJA) events in the future time-slice (Figure 5). It may be the case that these intense storms may become smaller in extent, below this paper's definition of "widespread". In comparison, the SIMOBS run shows a more equal distribution of events across the seasons, though it still remains within the variability of the seasonal totals for the RCM-based baseline outputs except in autumn (SON). However, Chen et al. (2021) suggests, using the UKCP18 Local projections (which uses convection-permitting models rather than RCMs), that convective storms in future may cover a greater area. Thus future work could look more specifically at differences in the methods which coud cause these differences.

A pairwise analysis suggested that inundated locations were asymptotically independent beyond a radius of around 120 km, but the distribution of dependence was slightly less concentrated in the future.

On the whole, the results suggest an increase in seasonality in widespread flood events, with more widespread flooding in winter, and possibly a shift towards smaller intense flooding in spring and summer. However, this approach cannot distinguish between flooding drivers such as convective storms, and so it is difficult to say what could cause such a change in the model. As mentioned above, the use of convection-permitting models (Chen et al., 2020) may prove useful in drawing out such differences and highlighting likely changes in flooding drivers.

Several potentially simultaneous but disjoint events were captured in the event sets, which may be due to capturing two consecutive or overlapping events due to the method of event length determination. Brunner et al. (2020) make use of a spatial dependence function (F-madogram) and hierarchical clustering to determine events for which points are mutually dependent to a sufficient degree. This would be an interesting direction to go in to improve event identification. To highlight spatial dependence in a simpler way than χ, Berghuijs et al. (2019) use a metric of flood "synchrony", measuring how often extreme floods occur at the same time within a given radius of a target point. The gridded data set we have available here could be evaluated using this metric, or one like it.

6 Conclusions

This paper has used UKCP18 Regional Projections and the Grid-to-Grid (G2G) hydrological model to generate a set of widespread flood events to investigate changes in spatial structure of river flooding in mainland Great Britain between the 1990s and 2060s. In summary, the number of widespread events (based on a POT2 threshold derived from 1980-2010 data)

was found to increase in total in the future time-slice, but was slightly lower in the future for spring and summer (March-August) events. On the whole, the results suggest an increase in seasonality in widespread flood events, with more widespread flooding in winter, and possibly a shift towards smaller intense flooding in spring and summer.

This paper and the data generated therein forms the basis for a wider scheme of work generating extreme flooding events for risk analysis, which is the subject of a number of subsequent papers: Griffin et al., (2022b) discussing statistical methods to generate large numbers of plausible widespread events with long return periods and Sayers et al., (2023) on applying the event sets to risk analysis through catastrophe modelling methods. Further work could look at more sophisticated methods of event identification, and look at describing or separating simultaneous or temporally-overlapping events. This work focuses on fluvial flooding but surface water flooding (not from inundation of rivers and water bodies) is also a large factor in estimating economic losses due to flooding. It would be of interest to use the Grid-to-Grid model including surface water (Rudd et al., 2020) applied to the framework of this paper to see if the different types of flooding will change in different ways over time.

Data availability

Peak flow data freely available from UK National River Flow Archive (nrfa.ceh.ac.uk). UKCP18 data available from Met Office under and Open Government Licence. Event set can be found at the Environmental Informatics Data Centre (Griffin et al., 2022a).

Author Contributions

ES and PS managed the project, AK and VB ran the hydrological modelling, AG ran the event extraction and summary, and performed the statistical analysis. All authors assisted in writing and editing the manuscript.

Acknowledgements

Funding for the project was provided through the UK Climate Resilience Programme supported by UK Research and Innovation and the UK Met Office.

References

Barker, L., Hannaford, J., Muchan, K., Turner, S. and Parry, S. (2016). The winter 2015/2016 floods in the UK: a hydrological appraisal. Weather, 71: 324-333. doi:10.1002/wea.2822

Bell, V.A., Kay, A.L., Jones, R.G., Moore, R.J. (2007a). Development of a high-resolution grid-based river flow model for use with regional climate model output. Hydrol. Earth Syst. Sci. 11 (1), 532–549. doi:10.5194/hess-11-532-2007

Bell, V.A., Kay, A.L., Jones, R.G., Moore, R.J. (2007b). Use of a grid-based hydrological model and regional climate model outputs to assess changing flood risk. Int. J. Climatol. 27, 1657–1671. doi:10.1002/joc.1539

Bell V.A., Kay A.L., Jones R.G. et al. (2009). Use of soil data in a grid-based hydrological model to estimate spatial variation in changing flood risk across the UK. J. Hydrol. 377(3–4): 335–350. doi:10.1016/j.jhydrol.2009.08.031

Bell, V. A., Kay, A. L., Cole, S. J., Jones, R. G., Moore, R. J., & Reynard, N. S. (2012). How might climate change affect river flows across the Thames Basin? An area-wide analysis using the UKCP09 Regional Climate Model ensemble. Journal of Hydrology, 442, 89-104.

Blöschl, G., Hall, J., Parajka, J., Perdigão, R. A. P., Merz, B., Arheimer, B., Aronica, G. T., Bilibashi, A., Bonacci, O., Borga, M., Čanjevac, I., Castellarin, A., Chirico, G. B., Claps, P., Fiala, K., Frolova, N., Gorbachova, L., Gül, A., Hannaford, J., … Živković, N. (2017). Changing climate shifts timing of European floods. Science, 357(6351), 588–590. doi:10.1126/science.aan2506

Chen Y, Paschalis A, Kendon E, Kim D, Onof C (2020). Changing spatial structure of summer heavy rainfall, using convection-permitting ensemble. Geophysical Research Letters, 48, e2020GL090903. doi: 10.1029/2020GL090903.

Coles, S. (2001). An Introduction to Statistical Modeling of Extreme Values. Springer London. doi:10.1007/978-1-4471-3675-0

Collet, L., Harrigan, S., Prudhomme, C., Formetta, G., & Beevers, L. (2018). Future hot-spots for hydro-hazards in Great Britain: A probabilistic assessment. Hydrology and Earth System Sciences Discussions, 1–22. doi:10.5194/hess-2018-274

Davies, H., Bell, V. (2008). Assessment of methods for extracting low resolution river networks from high resolution digital data. Hydrol. Sci. J. 54 (1), 17–28. doi:10.1623/hysj.54.1.17

De Luca, P., Hillier, J. K., Wilby, R. L., Quinn, N. W., Harrigan, S. (2017). Extreme multi-basin flooding linked with extra-tropical cyclones. Environmental Research Letters, 12(11), 114009. doi:10.1088/1748-9326/aa868e

Environment Agency (2011). The risk of widespread flooding – Capturing spatial patterns in flood risk from rivers and coasts. Science Report SC060088/R3. Bristol.

Filipova, V., Lawrence, D., Skaugen, T. (2019) A stochastic event-based approach for flood estimation in catchments with mixed rainfall and snowmelt flood regimes. Natural Hazards and Earth System Sciences, 19(1), 1-18. doi:10.5194/nhess-19-1-2019

Fuller, R.M., Smith, G.M., Sanderson, J.M., Hill, R.A., Thomson, A.G. (2002). The UK Land Cover Map 2000: Construction of a Parcel-Based Vector Map from Satellite Images, The Cartographic Journal, 39:1, 15-25, doi:10.1179/caj.2002.39.1.15

Griffin, A.; Kay, A.; Bell, V.; Stewart, E.J.; Sayer, P.; Carr, S. (2022a). Peak flow and probability of exceedance data for Grid-to-Grid modelled widespread flooding events across mainland GB from 1980-2010 and 2050-2080. NERC EDS Environmental Information Data Centre. doi:10.5285/26ce15dd-f994-40e0-8a09-5f257cc1f2ab

Griffin, A., Kay A., Stewart, E., Sayers, P., Carr, S. (2022b). Spatially coherent statistical simulation of widespread flooding events under climate change. Hydrology Research. 1 November 2022; 53 (11): 1428–1440. doi: doi:10.2166/nh.2022.069

Grossi, P., & Kunreuther, H. (2005) Catastrophe Modeling: A New Approach to Managing Risk (Vol. 25). Springer Science & Business Media.

Guillod, B. P., Jones, R. G., Dadson, S. J., Coxon, G., Bussi, G., Freer, J., Kay, A. L., Massey, N. R., Sparrow, S. N., Wallom, D. C. H., Allen, M. R., Hall, J. W. (2018). A large set of potential past, present and future hydro-meteorological time series for the UK. Hydrology and Earth System Sciences, 22, pp.611–634. doi:10.5194/hess-22-611-2018

Hosking, J., Wallis, J. (1997). Regional Frequency Analysis: An Approach Based on L-Moments. Cambridge: Cambridge University Press. doi:10.1017/CBO9780511529443

Hough, M. N., Jones, R. J. A. (1997). The United Kingdom Meteorological Office rainfall and evaporation calculation system: MORECS version 2.0-an overview. Hydrology and Earth System Sciences, 1(2), pp.227-239. doi:10.5194/hess-1-227-1997

HM Government, 2020. National Risk Register: 2020 edition. Cabinet Office: London.

Jimenez-Cisneros, B. (2015). Responding to the challenges of water security: The Eighth Phase of the International Hydrological Programme, 2014–2021. Proceedings of the International Association of Hydrological Sciences, 366, 10–19. doi:10.5194/piahs-366-10-2015

Jones, M. R., Blenkinsop, S., Fowler, H. J., Kilsby, C. G. (2014). Objective classification of extreme rainfall regions for the UK and updated estimates of trends in regional extreme rainfall. International Journal of Climatology, 34(3), pp.751-765. doi:10.1002/joc.3720

Lane, R. A., & Kay, A. L. (2021). Climate Change Impact on the Magnitude and Timing of Hydrological Extremes Across Great Britain. Frontiers in Water, 3, 684982. doi:10.3389/frwa.2021.684982

Kay A.L. (2021) Simulation of river flow in Britain under climate change: Baseline performance and future seasonal changes. Hydrological Processes. 35, e14137. doi:10.1002/hyp.14137

Kay, A.L. (2022) Differences in hydrological impacts using regional climate model and nested convection-permitting model data. *Climatic Change*, 173(1-2), 11, doi:10.1007/s10584-022-03405-z.

Kay, A. L., Lane, R. A., & Bell, V. A. (2022). Grid-based simulation of soil moisture in the UK: Future changes in extremes and wetting and drying dates. Environmental Research Letters, 17(7), 074029. https://doi.org/10.1088/1748-9326/ac7a4e

Kay, A. L., Griffin, A., Rudd, A. C., Chapman, R. M., Bell, V. A., Arnell, N. W. (2021). Climate change effects on indicators of high and low river flow across Great Britain. Advances in Water Resources, 151, 103909. doi:10.1016/j.advwatres.2021.103909

Kelder, T., Müller, M., Slater, L. J., Marjoribanks, T. I., Wilby, R. L., Prudhomme, C., Bohlinger, P., Ferranti, L., Nipen, T. (2020). Using UNSEEN trends to detect decadal changes in 100-year precipitation extremes. npj Climate and Atmospheric Science, 3(1), 47. doi:10.1038/s41612-020-00149-4

Met Office, Hollis, D (2019). Had UK-Grid Gridded Climate Observations on a 1km grid over the UK, v1.0.0.0 (1862–2017). Centre for Environmental Data Analysis, November 2019. doi:10.5285/2a62652a4fe6412693123dd6328f6dc8.

Morris, D.G. and Flavin, R.W. (1990). A digital terrain model for hydrology. Proc 4th International Symposium on Spatial Data Handling. Vol 1 Jul 23-27, Zürich, pp 250-262.

Murphy J, Harris G, Sexton D, Kendon E, Bett P, Clark R and Yamazaki K (2019). UKCP18 land projections: science report. Met Office: Exeter. www.metoffice.gov.uk/pub/data/weather/uk/UKCP18/science-reports/UKCP18-land-report.pdf [accessed Nov 2021]

Murphy, J. M., Harris, G. R. (2018). UKCP18 Land Projections: Science Report. Met Office Hadley Centre, Exeter.

National River Flow Archive (NRFA), 2020. https://nrfa.ceh.ac.uk [accessed Sep 2021]

Osborn, T.J. and Hulme M. (2002). Evidence for trends in heavy rainfall events over the UK. Phil. Trans. R. Soc. A. 360, pp.1313–1325. doi:10.1098/rsta.2002.1002

Paz, A. R., Collischonn, W., & Lopes da Silveira, A. L. (2006). Improvements in large-scale drainage networks derived from digital elevation models: TECHNICAL NOTE. Water Resources Research, 42(8). doi:10.1029/2005WR004544

Price, D., Pilling, C., Robbins, G., Lane, A., Boyce, G., Fenwick, K., Moore, R.J., Coles, J., Harrison, T., and Van Dijk, M. 2012. Representing the spatial variability of rainfall for input to the G2G distributed flood forecasting model: operational experience from the Flood Forecasting Centre. In: Moore, R.J.; Cole, S.J.; Illingworth, A.J., (eds.) Weather Radar and Hydrology, Proc. Exeter Symp., April 2011. International Association of Hydrological Sciences, 532-537. (IAHS Publ., 351).

Rudd, A.C., Kay, A.L., Wells, S.C., Aldridge, T., Cole, S.J., Kendon, E.J. and Stewart, E.J. (2020). Investigating potential future changes in surface water flooding hazard and impact. Hydrological Processes, 34, 139-149, doi:10.1002/hyp.13572.

Robson, A. J., & Reed, D. W. (1999). Statistical procedures for flood frequency estimation. In Flood Estimation Handbook (Vol. 3, p. 338). Institute of Hydrology.

Sayers, P.B., Horritt, M., Carr, S., Kay, A., Mauz, J., Lamb R., and Penning-Rowsell E. (2020). Third UK Climate Change Risk Assessment (CCRA3): Future flood risk. Published by Committee on Climate Change, London.

Sayers, P.B.; Griffin, A., Lowe, J., Bernie, D., Carr, S., Kay, A. and Stewart, E.J. (2023, in submission) Beyond the climate uplift – The importance of accounting for changes in the spatial structure of future fluvial flood events on flood risk in Great Britain. Submitted to Nature Climate Change.

Tanguy, M.; Dixon, H.; Prosdocimi, I.; Morris, D.G.; Keller, V.D.J. (2019). Gridded estimates of daily and monthly areal rainfall for the United Kingdom (1890-2017) [CEH-GEAR]. NERC Environmental Information Data Centre. doi:10.5285/ee9ab43d-a4fe-4e73-afd5-cd4fc4c82556

Tawn, J.A., Towe, R.P., Eastoe, E., Lamb, R. (2018). Modelling the clustering of extreme events for short-term risk assessment. Journal of Agricultural, Biological, and Environmental Statistics, *25*(1), pp.32–53 doi:10.1007/s13253-019-00376-0

Tawn, J.A., Shooter, R., Towe, R.P., Lamb, R. (2018) Modelling spatial extreme events with environmental applications. Spatial Statistics, *28*, pp.39–58. doi:10.1016/j.spasta.2018.04.007

Towe, R.P., Tawn, J.A., Lamb, R., Sherlock, C. (2019). Model-based inference of conditional extreme value distributionswith hydrological applications. Environmetrics. 2019; 30:e2575. doi:10.1002/env.2575